

QUT Digital Repository:
<http://eprints.qut.edu.au/>



Frost, Ray L. and Palmer, Sara J. and Spratt, Henry J. (2009) *Synthesis and Raman spectroscopic study of Mg/Al,Fe hydrotalcites with variable cationic ratios*. Journal of Raman Spectroscopy, 40(9). pp. 1138-1143.

© Copyright 2009 John Wiley and Sons

33
34
35
36
37
38
39
40
41
42
43
44
45
46
47
48
49
50
51
52
53

Hydrotalcites, or layered double hydroxides (LDHs) are fundamentally anionic clays, and are less well-known than cationic clays like smectites^{1,2}. The structure of hydrotalcite can be derived from a brucite structure (Mg(OH)₂) in which e.g. Al³⁺ or Fe³⁺ (pyroaurite-sjögrenite) substitutes for the Mg²⁺. This substitution creates a positive layer charge on the hydroxide layers, which is compensated by interlayer anions or anionic complexes^{3,4}. When LDHs are synthesised any appropriate anion can be placed in the interlayer. These anions may be any anion with a suitable negative charge including the carbonate anion. The hydrotalcite may be considered as a gigantic cation, which is counterbalanced by anions in the interlayer. In hydrotalcites a broad range of compositions are possible of the type [M²⁺_{1-x}M³⁺_x(OH)₂][Aⁿ⁻]_{x/n}.yH₂O, where M²⁺ and M³⁺ are the di- and trivalent cations in the octahedral positions within the hydroxide layers, with x normally between 0.17 and 0.33. It is normal practice to determine the composition of the formed hydrotalcite by chemical means such as ICP-AES or EDAX techniques. Aⁿ⁻ is an exchangeable interlayer anion⁵. In the natural hydrotalcites reevesite and pyroaurite, the divalent cations are Ni²⁺ and Mg²⁺ respectively with the trivalent cation being Fe³⁺. In these cases, the carbonate anion is the major interlayer counter anion. Normally the hydrotalcite structure based upon takovite (Ni,Al) and hydrotalcite (Mg,Al) has basal spacings of ~8.0 Å where the interlayer anion is carbonate. Reevesite and pyroaurite are based upon the incorporation of carbonate into the interlayer with d(003) spacings of around 8 Å^{6,7}.

54
55
56
57
58
59
60
61
62
63
64
65

The reason for the potential application of hydrotalcites as catalysts rests with the ability to make mixed metal oxides at the atomic level, rather than at a particle level. Such mixed metal oxides are formed through the thermal decomposition of the hydrotalcite^{8,9}. There are many other important uses of hydrotalcites such as in the removal of environmental hazards in acid mine drainage^{10,11}, and a mechanism for the disposal of radioactive wastes¹². Their ability to exchange anions presents a system for heavy metal removal from contaminated waters¹³. The study of minerals, including hydrotalcites, by Raman spectroscopy has proven to be very useful¹⁴⁻²³. Indeed, Raman spectroscopy has proven most useful for the study of diagenetically related minerals as often occurs with hydrotalcite minerals. Some previous studies have been undertaken by the authors using Raman spectroscopy to study hydrotalcites. Spectroscopic studies, especially Raman studies, of hydrotalcites are limited especially where large anions are involved. The aim of this paper is

66 to present Raman and infrared spectra of planned hydrotalcites with carbonate in the
67 interlayer.

68

69 In this work, we report the synthesis of Mg/Al,Fe hydrotalcites with variable Mg/Al
70 cation ratio. These synthetic materials are to be used to characterise hydrotalcites that form
71 in Al³⁺ and Fe³⁺ rich solutions, such as in the Bayer industry. We also report the Raman and
72 infrared spectroscopic analysis of hydrotalcite and explore the effect of divalent/trivalent
73 ratio on hydrotalcite formation.

74

75 **EXPERIMENTAL**

76

77 **Preparation of Mixed Metal Ion Solution**

78

79 Varying amounts of aluminium chloride hexahydrate, iron(III) chloride hexahydrate and
80 magnesium chloride hexahydrate are dissolved in 500 mL of water. The ratio of moles of M²⁺
81 to M³⁺, where M is a metal cation, in the different solutions is 2:1, 3:1 and 4:1. The following
82 Table summarises how much of each metal is dissolved in 500 mL of water. A caustic
83 solution is also prepared, containing 2 M of sodium hydroxide and 0.2 M of sodium
84 carbonate.

85

86

87 **Insert Table 1 here**

88

89 The chosen metal ion solution is then added at 40 mL/minute via a peristaltic pump. The
90 combined solutions are then vacuum filtered, washed thoroughly with hot degassed water and
91 dried in an oven overnight at 120 °C.

92

93 **X-ray diffraction**

94

95 X-Ray diffraction patterns of powdered samples are collected using a Philips X'pert wide
96 angle X-Ray diffractometer, operating in step scan mode, with Co K α radiation (1.78897Å).

97

98 **Raman microscopy**

99

100 The crystals of hydrotalcite are placed on the stage of an Olympus BHSM microscope,
101 equipped with 10x and 50x objectives and are part of a Renishaw 1000 Raman microscope
102 system, which also includes monochromators, a filter system and a charge coupled device
103 (CCD). Raman spectra were excited by a HeNe laser (633 nm) at a nominal resolution of 2
104 cm^{-1} in the range between 100 and 4000 cm^{-1} . Repeated acquisition using the highest
105 magnification is accumulated to improve the signal to noise ratio. Spectra are calibrated using
106 the 520.5 cm^{-1} line of a silicon wafer. Previous studies by the authors provide more details of
107 the experimental technique²⁴⁻²⁹.

108

109 **Infrared spectroscopy**

110

111 Infrared spectra are obtained using a Nicolet Nexus 870 FTIR spectrometer with a
112 smart endurance single bounce diamond ATR cell. Spectra over the 4000-525 cm^{-1} range are
113 obtained by the co-addition of 128 scans with a resolution of 4 cm^{-1} and a mirror velocity of
114 0.6329 cm/s.

115

116 Spectral manipulation such as baseline adjustments, smoothing and normalisation are
117 performed using the GRAMS® software package (Galactic Industries Corporation, Salem,
118 NH, USA). Band component analysis is undertaken using the Jandel 'Peakfit' software
119 package, which enables the type of fitting function to be selected and allows specific
120 parameters to be fixed or varied accordingly. Band fitting is achieved using a Lorentz-Gauss
121 cross-product function with the minimum number of component bands used for the fitting
122 process. The Lorentz-Gauss ratio was maintained at values greater than 0.7 and fitting is
123 undertaken until reproducible results were obtained with squared correlations of r^2 greater
124 than 0.995.

125

126

127 **RESULTS AND DISCUSSION**

128

129 **X-ray diffraction**

130

131 The X-ray diffraction patterns for the carbonate interlayered hydrotalcites are shown in Fig.
132 1. EDX determined the hydrotalcite ratios to be 1.7, 2.7 and 4.0 for the 2:1, 3:1 and 4:1

133 hydrotalcites respectively. The XRD patterns prove that the hydrotalcites have been
134 successfully synthesised. Hydrotalcite normally has a d(003) spacing of around 7.9 Å. The
135 sulphate interlayered hydrotalcite has a spacing of 8.0 Å. There is an apparent small shift to
136 higher d(003) spacings as the cation ratio increases. The greatest shift is observed when
137 comparing the 2:1 HT with the 3:1 HT. The results obtained by EDX found that the Fe:Al
138 concentration decreased as the overall Mg/Al,Fe ratio increased. It is not clearly understood
139 as to why the change in cation ratio caused an increase in the d(001) spacing. Thus the XRD
140 patterns show that the d-spacing for the carbonate interlayered hydrotalcite is cation
141 dependent.

142

143 **Vibrational spectroscopy**

144

145 Only a very limited number of Raman studies have been reported so far on the
146 interlayer carbonate anion in hydrotalcites. There are many examples of naturally occurring
147 hydrotalcites with carbonate as the interlayer anion. When the carbonate species is present as
148 a free ion, not involved in any bonding, it will exhibit a space group of D_{3h} . In the Raman
149 spectrum one will observe $\nu_1(A'1)$, $\nu_3(E')$ and $\nu_4(E')$. As a result three bands, the bending
150 non-planar mode $\nu_2(A''2)$, the anti-symmetrical stretching mode $\nu_3(E')$ and the bending
151 angular mode $\nu_4(E')$, will be observed in the infrared spectrum around 880, 1415 and 680 cm^{-1} ,
152 while the symmetric stretching mode $\nu_1(A'1)$ is infrared inactive. However, changes can be
153 expected when the carbonate ion is intercalated in the hydrotalcite structure as it will be
154 affected by interactions with interlayer water molecules and/or OH-groups from the
155 hydrotalcite layers. In comparison with free CO_3^{2-} a shift towards lower wavenumbers is
156 generally observed. Interaction between interlayer water molecules and the carbonate ion is
157 reflected by the appearance of bands at around 3000-3100 cm^{-1} , in the OH-stretching region
158 of the infrared spectrum around 3000-3100 cm^{-1}

159

160 The Raman and infrared spectra may be conveniently divided into sections according
161 to where the various vibrational bands are found. Thus the spectra are sectioned into (a) the
162 OH stretching region, (b) the CO_3^{2-} stretching region and (c) the CO_3^{2-} bending region. The
163 Raman and infrared spectra of the OH stretching region are displayed in Figs. 2 and 3
164 respectively. The spectra in these two figures may be contrasted. Water bands are not so
165 easily observed in the Raman spectra of these hydrotalcites as water is a very poor Raman

166 scatterer. The intensity of the bands in Fig. 2 is therefore more likely to be associated with
167 OH stretching bands. The intensity of the spectral profile in the infrared spectra is more
168 likely to be associated with water stretching vibrations. The spectral profile is shifted to
169 lower wavenumbers in the infrared spectrum. The Raman spectral profiles for the 2:1, 3:1
170 and 4: 1 are different. The peak maximum for the 2:1 hydrotalcite occurs at around 3513 cm⁻¹.
171 The bands at 2908, 3094 and 3360 cm⁻¹ are assigned to water stretching bands. The first
172 band at 2908 cm⁻¹ is attributed to water which is strongly hydrogen bonded to the carbonate
173 anion. Such a unit is held within the hydrotalcite interlayer and serves to stabilise the
174 hydrotalcite structure. The Raman bands for the 2:1 HT at 3513, 3592 and 3656 cm⁻¹ are
175 attributed to OH stretching vibrations of OH units bonded to the cations of the brucite-layer.
176 The combined intensities of the two Raman bands at around 3600 cm⁻¹, increases as the
177 divalent/trivalent cation ratio increases. It is proposed that the increase in intensity is due to a
178 larger quantity of M-OH bonds within the structure, where M can be Mg, Al, Fe, or any
179 permutation of these metals. A shift of the overall band profile to higher wavenumbers, as the
180 cation ratio increases, is believed to be due to an increase in the quantity of Mg-OH bonds.
181 Therefore, changes in the cationic ratio changes the Raman spectral profile in the OH
182 stretching region.

183

184 In the infrared spectra of the OH stretching region (Fig.3) changes in the spectral
185 profile are observed for the different hydrotalcites synthesised. The infrared bands for the 2:1
186 HT at 3074, 3275 and even 3439 cm⁻¹ are assigned to water stretching bands. The higher
187 wavenumber band at 3588 cm⁻¹ may be attributed to the OH stretching bands of the Mg₃OH
188 and Al₃OH units. The intensity of the bands at 3471 and 3596 cm⁻¹ increase for the 3:1 HT.
189 The intensity of the higher two wavenumber bands increases for the 4:1 HT. It is suggested
190 that the two bands at 3043 and 3313 cm⁻¹ for the 3:1 HT and at 3064 and 3337 cm⁻¹ are due to
191 water in two different environments in the HT interlayer. The lower wavenumber band is
192 attributed to water which is reasonably strongly hydrogen bonded, possibly bonded to
193 carbonate in the hydrotalcite interlayer.

194

195 An estimate of the intensity of the OH stretching vibrations may be obtained by an
196 assessment of the type and number of MOH vibrations. In brucite type solids, there are
197 tripod units M₃OH with several metals such as M, M', M''. In hydrotalcites such as those
198 based upon Mg and Zn of formula Mg_xZn_{6-x}Al₂(OH)₁₆(CO₃).4H₂O, a number of statistical
199 permutations of the M₃OH units are involved. These are Mg₃OH, Zn₃OH, Al₃OH and

200 combinations such as Mg_2ZnOH , Zn_2MgOH , Mg_2AlOH , Al_2MgOH , Al_2ZnOH , Zn_2AlOH ,
201 and even $MgZnAlOH$. These types of units will be distributed according to a probability
202 distribution according to the composition. In this model, a number of assumptions are made,
203 namely that the molecular assembly is random and that no islands or lakes of cations are
204 formed. Such assembly is beyond the scope of this work but needs to be thoroughly
205 investigated. In the simplest case namely $Mg_6Al_2(OH)_{16}(CO_3) \cdot 4H_2O$ the types of units would
206 be Mg_3OH , Mg_2AlOH , $MgAl_2OH$ and Al_3OH . A similar situation would exist for the
207 $Mg_6Fe_2(OH)_{16}(CO_3) \cdot 4H_2O$ hydrotalcite. In a somewhat oversimplified model, for the
208 $Mg_6Fe_2(OH)_{16}(CO_3) \cdot 4H_2O$ hydrotalcite, the most intense bands would be due to the Mg_3OH
209 and Fe_3OH bands.

210

211 The Raman spectra of the synthesised hydrotalcites with different cationic ratios in
212 the 950 to 1650 cm^{-1} region are shown in Fig. 4. The band at around 1059 cm^{-1} is assigned to
213 the $(CO_3)^{2-}$ symmetric stretching mode. The band is not a simple band and may be
214 subdivided into component bands as shown. The additional components are more readily
215 observed in the Raman spectrum of the 4:1 HT. For the 2:1 HT three bands are observed at
216 1032 , 1060 and 1091 cm^{-1} . The 1032 cm^{-1} band is assigned to a ‘free’ carbonate anion i.e. a
217 carbonate anion which is not bonded to the brucite hydroxyl surface and water; the band at
218 1060 cm^{-1} is associated with carbonate anions bonded to the brucite hydroxyl surface; the
219 higher wavenumber band at 1091 cm^{-1} is attributed to carbonate anions strongly hydrogen
220 bonded to water. The three carbonate bands are found at 1022 , 1058 and 1083 cm^{-1} for the
221 3:1 HT. The bands are observed at 1022 , 1059 and 1076 cm^{-1} for the 4:1 HT. Bands
222 assigned to carbonate strongly hydrogen bonded to water shift to lower wavenumbers as the
223 cation ratio increases. This shift suggests that the bonding between carbonate and water is
224 becoming stronger as the hydrogen bond distances decrease. Low intensity bands are
225 observed in the 1200 to 1600 cm^{-1} region. For the 2:1 HT two bands are observed at 1212
226 and 1386 cm^{-1} ; for the 3:1 HT two bands are observed at 1226 and 1384 cm^{-1} and for the 4:1
227 HT two Raman bands are found at 1254 and 1375 cm^{-1} . One probable assignment of these
228 bands is to the $(CO_3)^{2-}$ antisymmetric stretching modes. The band at around 1588 cm^{-1} is
229 considered to be due to water bending modes. Because the intensity of these bands is quite
230 low, it is difficult to define exactly the position of these bands.

231

232 The infrared spectra of the three synthesised HTs are shown in Fig. 5. These spectra
233 compliment the Raman spectra reported in Fig. 4. Interestingly no $(CO_3)^{2-}$ symmetric

234 stretching modes are observed. The very low intensity bands in the 1200 to 1600 cm^{-1}
235 Raman spectral region show significantly greater intensity in the infrared spectrum. For the
236 2:1 HT two bands are observed at 1362 and 1413 cm^{-1} . For the 3:1 HT the bands are found
237 at 1364 and 1474 cm^{-1} and for the 4:1 HT the bands are observed at 1367 and 1446 cm^{-1} .
238 These bands are assigned to the $(\text{CO}_3)^{2-}$ antisymmetric stretching modes. The water bending
239 mode at around 1640 cm^{-1} is more easily observed in the infrared spectrum as water has a
240 very low scattering cross section in the Raman spectrum.

241
242 A comparison may be made with the band positions in other HTs and natural
243 carbonates. The shift towards lower wavenumbers indicates a loss of freedom compared to
244 free CO_3^{2-} and as a consequence a lowering of the carbonate symmetry occurs, from D_{3h} to
245 probably C_{2v} or C_v . The Raman spectrum of takovite displays intense Raman band at 1060
246 cm^{-1} with a low intensity band at 1042 cm^{-1} . The position of this band may be compared with
247 the values for witherite and cerrusite where positions of 1063 and 1053 cm^{-1} are observed.
248 The infrared spectrum of takovite shows two bands at 1351 and 1417 cm^{-1} . As a result of this
249 symmetry lowering the infrared inactive ν_1 mode will be activated. Indeed, a weak band has
250 been observed around 1050-1060 cm^{-1} . In addition the ν_3 mode shows a small splitting in the
251 order of 30-60 cm^{-1} . Some papers have only reported the activated ν_1 in combination with a
252 single ν_3 band. In these cases the ν_3 band seems to be broadened due to an overlap of the two
253 split modes ν_3 and ν_{3a} .

254
255 The Raman spectra in the 100 to 850 cm^{-1} region are shown in Fig. 6. The two bands
256 at around 471 and 548 cm^{-1} are common to all three spectra. The bands are considered to be
257 due to the linkage bonds, such as AlOAl and AlOMg linkage in the hydrotalcite. The bands
258 observed in the Raman spectra at around 691 cm^{-1} is assigned to the $(\text{CO}_3)^{2-}$ ν_4 mode. Since
259 the band is of low intensity, it is not possible to determine whether there is more than one
260 band present in this spectral region. These low intensity bands are observed more clearly in
261 the infrared spectrum (Fig. 5). For the 2:1 HT three infrared bands are noted at 604, 733 and
262 854 cm^{-1} ; for the 3:1 HT infrared bands are observed at 590 and 691 cm^{-1} and for the 4:1 HT
263 the bands are found at 576 and 673 cm^{-1} . These bands are assigned to the $(\text{CO}_3)^{2-}$ ν_4 mode.
264 For takovite a band is observed at 687 cm^{-1} and is attributed to the ν_4 mode. However, for the
265 ν_4 mode Klopogge and Frost reported a minor sharp band at 694 cm^{-1} , which indicates a
266 similar sized shift but in opposite direction. A reasonable explanation for this band is given

267 by Kagunya *et al.*, who showed the presence of a band at 698 and 695 cm⁻¹ in the Raman
268 spectra of Mg/Al-hydrotalcites with OH⁻ and CO₃²⁻ as interlayer anion, respectively and
269 assigned this vibration as the E_{g(T)} mode.³⁰ This band will then fully overlap the much
270 weaker carbonate ν₄ mode. Detailed examination of the 694 cm⁻¹ band indicates a rather
271 sudden broadening supporting an overlap between these two bands. Similarly, Kagunya *et al.*
272 gave an alternative assignment for the 1060 cm⁻¹ band as the E_{g(R)}(OH) mode, which they
273 observed in both the carbonate and the hydroxyl interlayered LDHs.³⁰

274

275 CONCLUSIONS

276

277 In this research we have shown that hydrotalcites with different cationic ratios
278 (Mg/Al,Fe) can be successfully synthesised. By comparison of the X-ray diffraction patterns
279 of the synthesised hydrotalcites with a standard reference pattern, it is proven that the
280 hydrotalcites were synthesised. It is observed in XRD that increasing the cation ratio causes
281 a change in the d₍₀₀₃₎ spacing due to the incorporation of the larger Fe³⁺ ions. The reason for
282 this change is not known. Hydrotalcites have a unique structure in that the mineral acts like
283 anionic clay with a 'giant' cation whose charge is counterbalanced by multiple anions in the
284 interlayer. Hydrotalcites are normally not easy to measure in terms of Raman spectroscopy
285 because of their small particle size together with their disordered nature.

286

287 In this work, both the Raman and infrared spectra of the interlayer anion of carbonate
288 have been collected and the spectra related to the structure of the synthesised mineral. The
289 hydroxyl stretching region of both Raman and infrared observed a shift and intensity changes,
290 due to the increased number of Mg-OH bonds in the hydrotalcite structure. The splitting of
291 the ν₃, ν₄ and ν₂ modes indicates symmetry lowering of the carbonate anions. The symmetry
292 lowering must be taken into account through the bonding of the carbonate anions to both
293 water and the brucite-like hydroxyl surface. Water plays an essential role in the hydrotalcite
294 structure as may be evidenced by the position of the water bending modes. The water is
295 strongly hydrogen bonded to both the anions and the hydroxyl surface. Raman spectroscopy
296 has the advantage of water being a very poor scatterer and hence is difficult to observe
297 compared with IR spectroscopy. Thus the cation OH stretching vibrations are more readily
298 observed with Raman spectroscopy.

299

300

301

302

303 **Acknowledgments**

304

305 The financial and infra-structure support of the Queensland University of

306 Technology, Inorganic Materials Research Program is gratefully acknowledged. . One of the

307 authors (SJP) is grateful to RioTintoAlcan International Limited for a Masters scholarship.

308 The Australian Research Council (ARC) is thanked for funding the instrumentation.

309

310

311 **REFERENCES**

- 312 1. Hashi K, Kikkawa S, Koizumi M *Clays and Clay Minerals* **1983**, *31*, 152-4.
313 2. Ingram L, Taylor HFW *Min. Mag.* **1967**, *36*, 465-79.
314 3. Taylor RM *Clay Minerals* **1982**, *17*, 369-72.
315 4. Taylor HFW *Min. Mag.* **1969**, *37*, 338-42.
316 5. Hansen HCB, Koch CB *App. Clay Sc.* **1995**, *10*, 5-19.
317 6. Bish DL, Livingstone A *Min. Mag.* **1981**, *44*, 339-43.
318 7. Nickel EH, Clarke RM *Am. Min.* **1976**, *61*, 366-72.
319 8. Rey F, Fornes V, Rojo JM *J. Chem. Soc., Faraday Trans.* **1992**, *88*, 2233-8.
320 9. Valcheva-Traykova M, Davidova N, Weiss A *J. Mater. Sci.* **1993**, *28*, 2157-62.
321 10. Lichti G, Mulcahy J *Chem. Aust.* **1998**, *65*, 10-13.
322 11. Seida Y, Nakano Y *J. Chem. Eng. Japan* **2001**, *34*, 906-911.
323 12. Roh Y, Lee SY, Elless MP, Foss JE *Clay. Clay Min.* **2000**, *48*, 266-271.
324 13. Seida Y, Nakano Y, Nakamura Y *Water Res.* **2001**, *35*, 2341-2346.
325 14. Frost RL, Cejka J, Ayoko G *J. Raman Spectrosc.* **2008**, *39*, 495-502.
326 15. Frost RL, Cejka J, Ayoko GA, Dickfos MJ *J. Raman Spectrosc.* **2008**, *39*, 374-379.
327 16. Frost RL, Cejka J, Dickfos MJ *J. Raman Spectrosc.* **2008**, *39*, 779-785.
328 17. Frost RL, Cejka J, Keeffe EC, Dickfos MJ *J. Raman Spectrosc.* **2008**, *39*, 1413-1418.
329 18. Frost RL, Dickfos MJ, Cejka J *J. Raman Spectrosc.* **2008**, *39*, 582-586.
330 19. Frost RL, Dickfos MJ, Cejka J *J. Raman Spectrosc.* **2008**, *39*, 1158-1161.
331 20. Frost RL, Dickfos MJ, Reddy BJ *J. Raman Spectrosc.* **2008**, *39*, 1250-1256.
332 21. Frost RL, Hales MC, Wain DL *J. Raman Spectrosc.* **2008**, *39*, 108-114.
333 22. Frost RL, Keeffe EC *J. Raman Spectrosc.* **2008**, *in press*.
334 23. Frost RL, Keeffe EC *J. Raman Spectrosc.* **2008**, *39*, 1408-1412.
335 24. Frost RL, Locke A, Martens WN *J. Raman Spectrosc.* **2008**, *39*, 901-908.
336 25. Frost RL, Reddy BJ, Dickfos MJ *J. Raman Spectrosc.* **2008**, *39*, 909-913.
337 26. Hales MC, Frost RL, Martens WN *J. Raman Spectrosc.* **2008**, *39*, 1141-1149.
338 27. Palmer SJ, Frost RL, Ayoko G, Nguyen T *J. Raman Spectrosc.* **2008**, *39*, 395-401.
339 28. Zhao Y, Frost RL *J. Raman Spectrosc.* **2008**, *39*, 1494-1501.
340 29. Zhao Y, Yang J, Frost RL *J. Raman Spectrosc.* **2008**, *39*, 1327-1331.
341 30. Kagunya W, Baddour-Hadjean R, Kooli F, Jones W *Chem. Phys.* **1998**, *236*, 225-234.

342
343
344

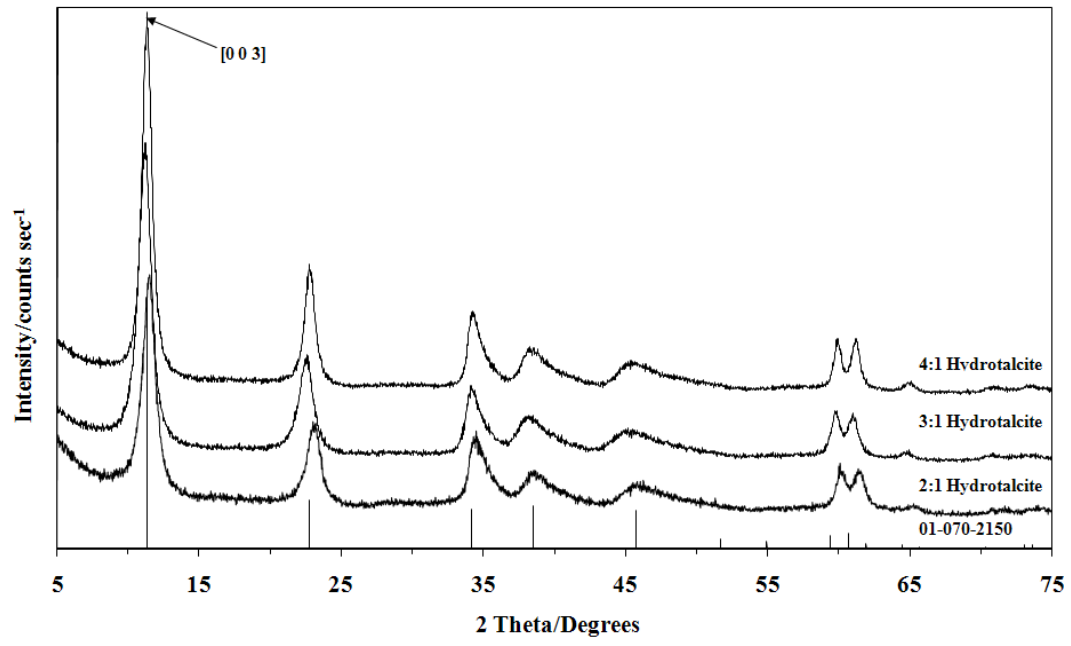
345

	<i>2:1 Solution</i>	<i>3:1 Solution</i>	<i>4:1 Solution</i>
<i>Magnesium</i>	67.765g	76.24g	81.32g
<i>Aluminium</i>	11.11g	8.335g	6.665g
<i>Iron(III)</i>	22.525g	16.895g	13.515g

346

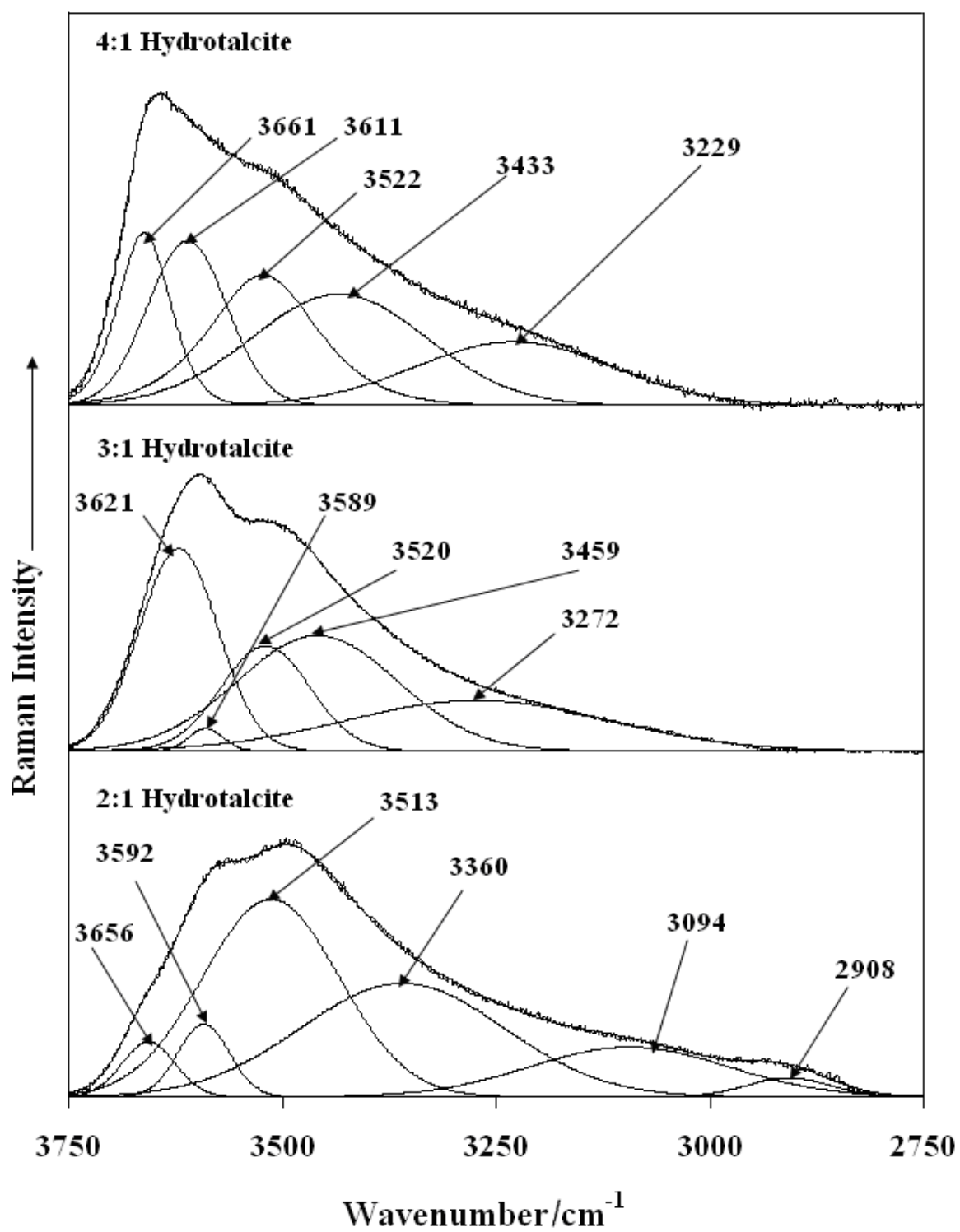
347 **Table 1**

348	List of Fig.s
349	
350	Fig. 1 X-ray diffraction patterns of the synthesised hydrotalcites with variable cationic ratios
351	
352	Fig. 2 Raman spectra of the synthesised hydrotalcites with variable cationic ratios in the 2750
353	to 3750 cm^{-1} region
354	
355	Fig. 3 Infrared spectra of the synthesised hydrotalcites with variable cationic ratios in the
356	2000 to 4000 cm^{-1} region
357	
358	Fig. 4 Raman spectra of the synthesised hydrotalcites with variable cationic ratios in the 950
359	to 1650 cm^{-1} region
360	
361	Fig. 5 Infrared spectra of the synthesised hydrotalcites with variable cationic ratios in the 500
362	to 1750 cm^{-1} region
363	
364	Fig. 6 Raman spectra of the synthesised hydrotalcites with variable cationic ratios in the 100
365	to 600 cm^{-1} region
366	

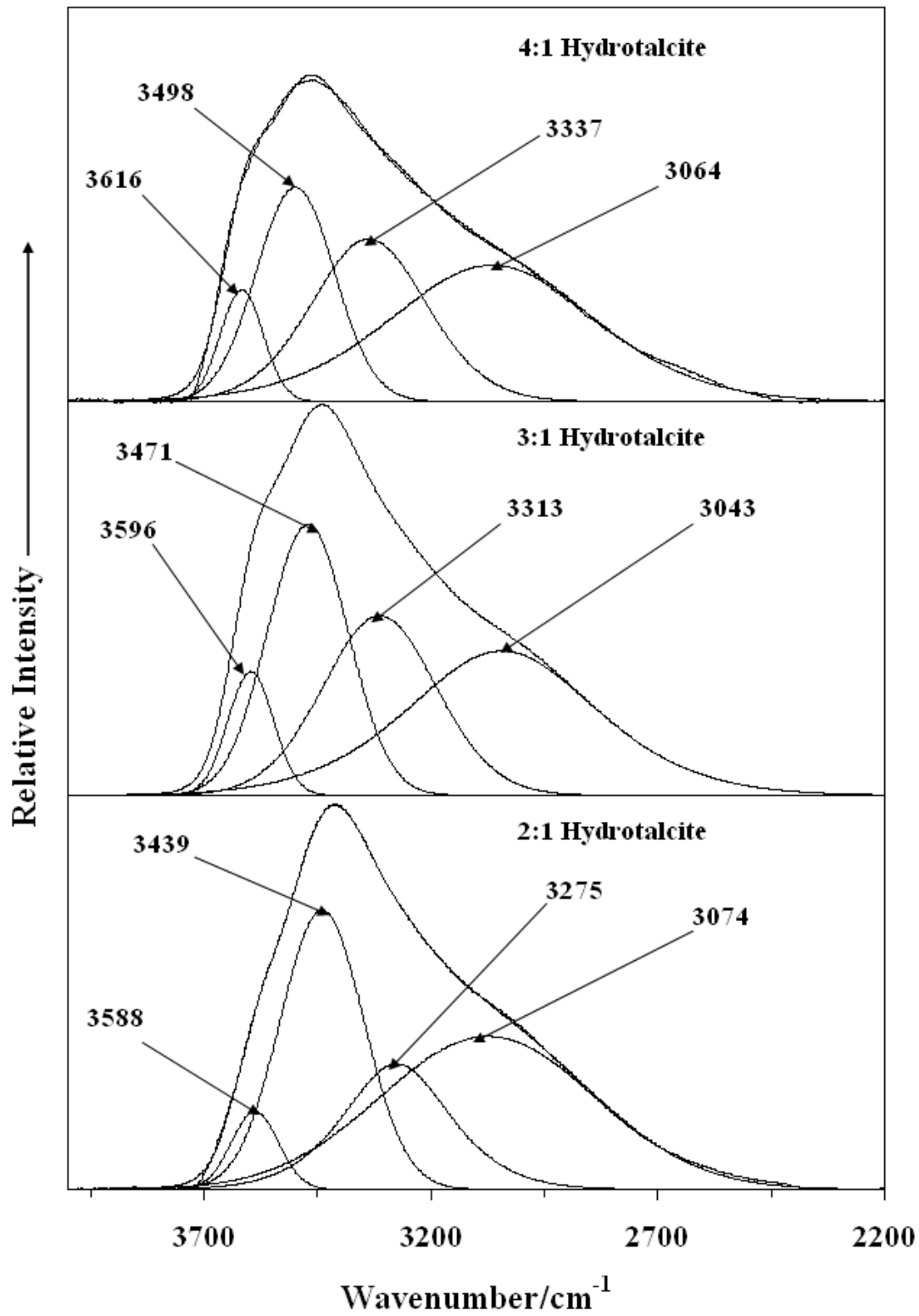


367
368
369
370

Fig. 1

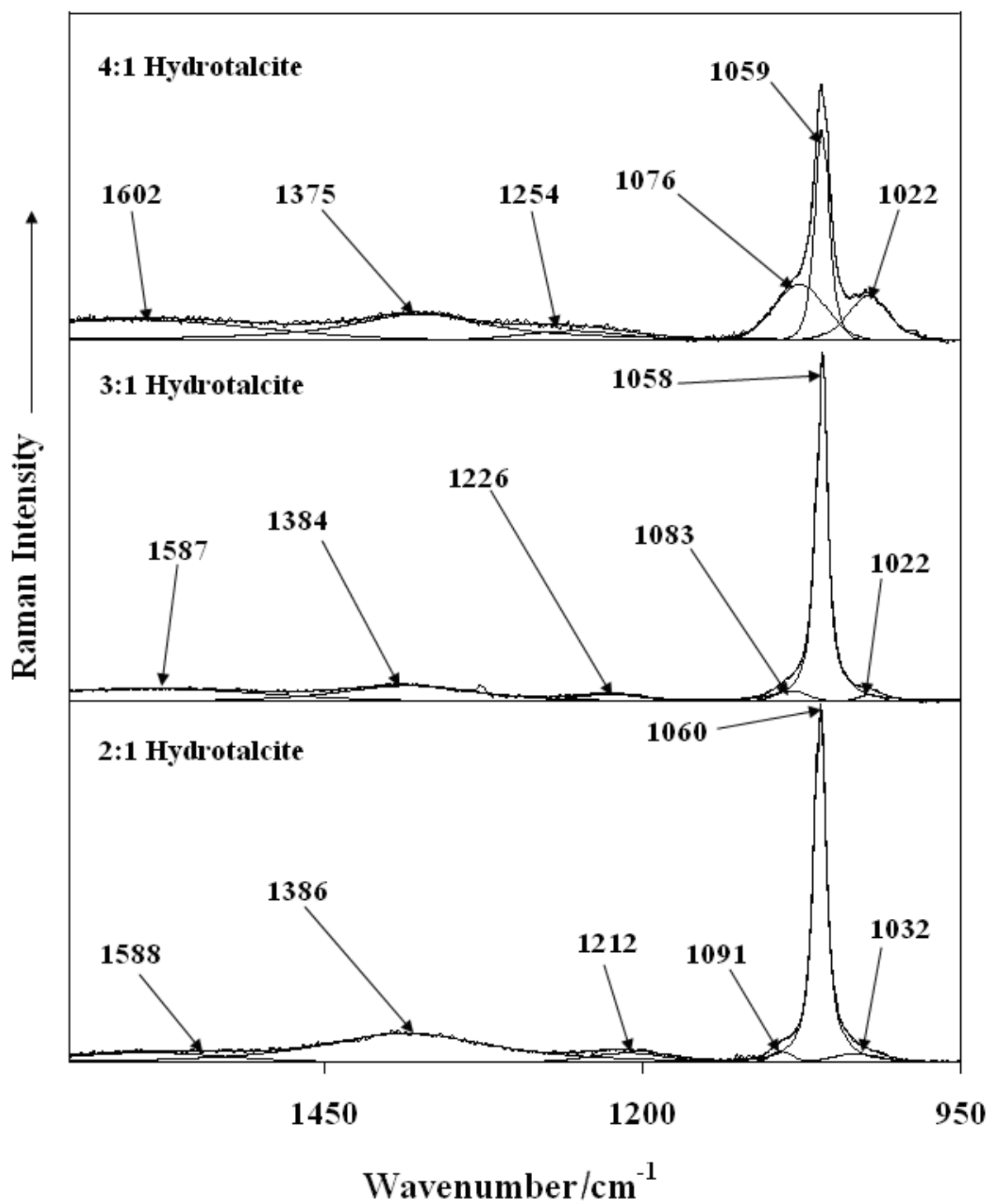


371
372 **Fig. 2**
373
374



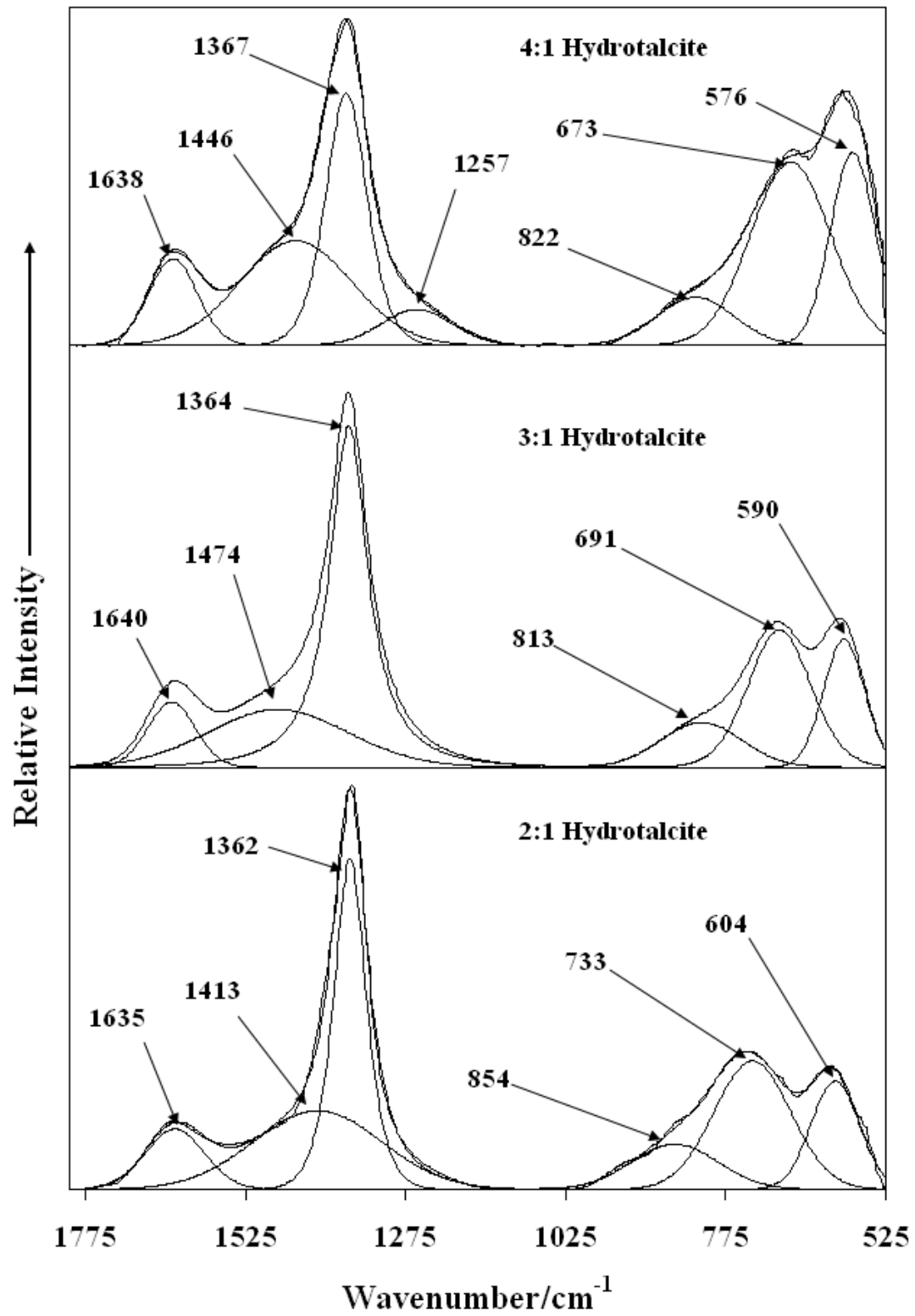
375
376
377

Fig. 3



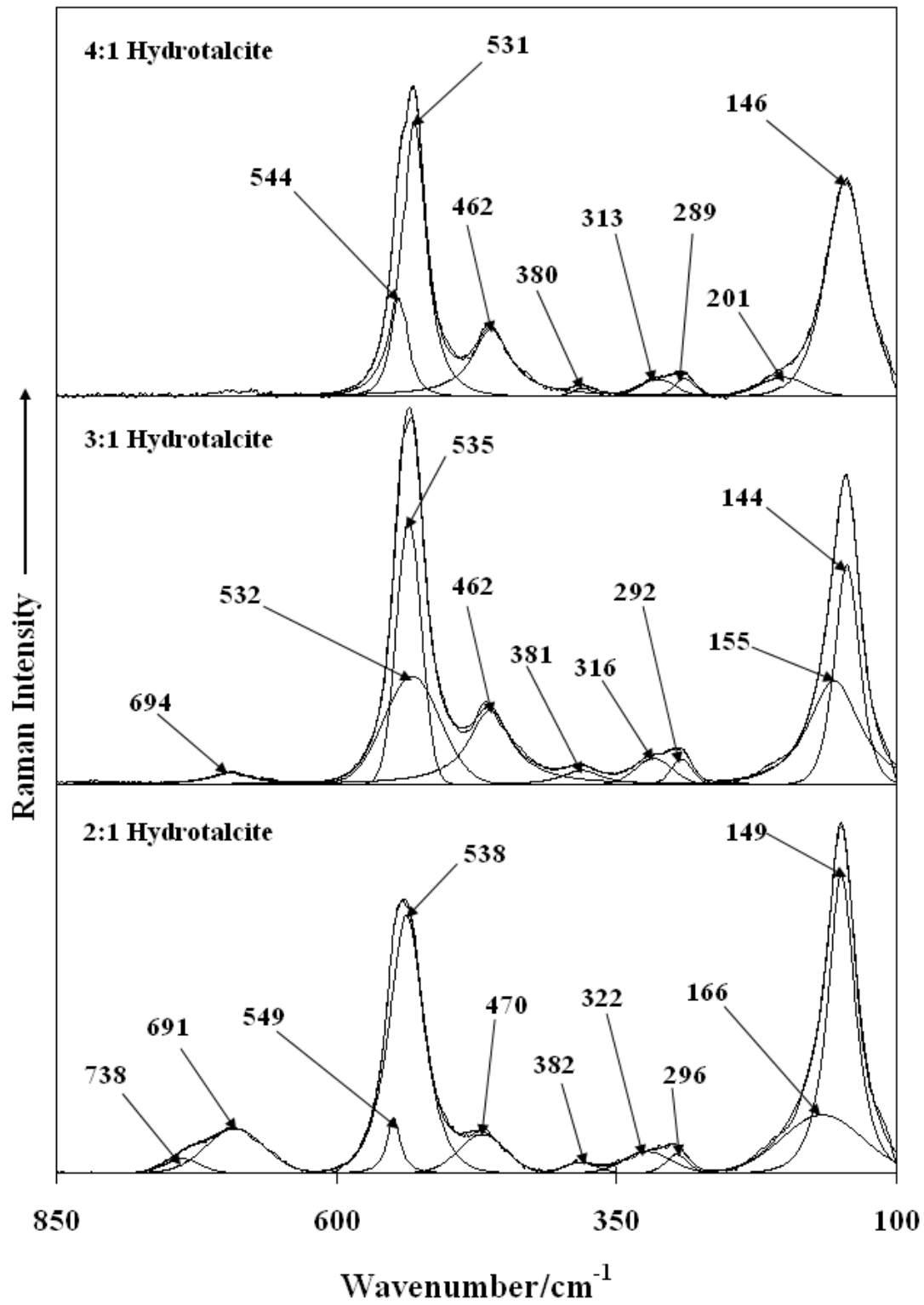
378
 379
 380
 381
 382

Fig. 4



383
384
385
386

Fig. 5



387
 388
 389
 390
 391

Fig. 6